Electronic Supplementary Material (ESI) for Physical Chemistry Chemical Physics.
This journal is © the Owner Societies 2021

Supplementary Information for

Tri-atomic Pt clusters induce the effective pathways in Co_{core}-Pd_{shell} Nanocatalyst surface for the high performance Oxygen Reduction Reaction

Haolin Li,[a,b] Kuan-Wen Wang,[c] Alice Hu,[a,d] Jyh-Pin Chou[e*] and Tsan-Yao Chen[b,f,g*]*

[a] *Department of Mechanical Engineering, City University of Hong Kong, Hong Kong, China*

[b] *Department of Engineering and System Science, National Tsing Hua University, Hsinchu 30013, Taiwan*

[c] *Institute of Materials Science and Engineering, National Central University, Taoyuan City 32001, Taiwan*

[d] *Department of Materials Science and Engineering, City University of Hong Kong, Hong Kong, China*

[e] *Department of Physics, National Changhua University of Education, Changhua, Taiwan*

[f] *Institute of Nuclear Engineering and Science, National Tsing Hua University, Hsinchu, Taiwan*

[g] *Department of Materials Science and Engineering, National Taiwan University of Science and Technology, Taipei, Taiwan*

*** Corresponding author**: (A. H) Email: alicehu@cityu.edu.hk; (J.-P. C) Email: jpchou@cc.ncue.edu.tw; (T.-Y. C) Email: tsanyao@mx.nthu.edu.tw

Supplementary Note 1 | Details about the stable initial-state (IS), transition-state (TS) and final-state (FS) geometries of the "O_2 dissociation" and "O* hydrogenation" stages on various models of interest.

Generally, it is believed that the most stable chemisorption configuration on metal is two-fold bridge site (i.e. M-b site) for O_2 molecule, three-fold hollow sites (i.e. M-h / f site, where h and f stand respectively for the hcp and fcc sites) for atomic O*, top site (i.e. M-t site) for H_2O molecule, and top / bridge site (i.e. M-t / M-b site) for OH radicals on a catalyst surface; where "M" is Pd or Pt atoms in this study.

In the first step the "O_2 dissociation", the chosen initial-state (IS) and final-state (FS) geometries are respectively an O_2 molecule adsorbing on a diatomic bridge site and then being split into two atomic O^{ads} that relocate onto two adjacent hollow sites. In the second step "the O* hydrogenation", the chosen IS and FS are one adsorbed O* atom on the hollow site interacting with a neighboring H_2O molecule adsorbed on a metal atom. The final product is two OH radicals. The transition-state (TS) structures (the highest NEB image) in the 1^{st} and 2^{nd} step reactions are respectively considered as the moments (i.e., the reaction energy barrier height) of O-O bond breakage and O-H bond formation.

In the Pt_n (n = 1-9, 16 and 32) model, the stable geometries for O_2 adsorption are set as the IS of the 1^{st} step. They are bridge sties in the edge region of the Pt-cluster (Pt-b^e). After splitting, the O* atoms will move to the two PtPd-h sites adjacent to the Pt-b^e. In the 2^{nd} step, the H_2O molecules are adsorbed atop the Pd atoms (Pd-t sites) in the peripheral Pd region for the subsequent O* hydrogenation. Atomic structures for the two-step pathways on various surfaces of the Pt_n are presented in Supplementary Fig. 4 and 5.

Supplementary Table 1 | The adsorption energies (E_{ads}, given in eV) of molecular oxygen (O_2) and atomic oxygen (O*) on different adsorption sites corresponding to the model catalysts of the Pd(111) and Pt_0 to Pt_4.

	O_2-site	E_{ads}	O*-site	E_{ads}
Pd(111)	Pd-b	−0.75	Pd-h	−1.15
			Pd-f	−1.34
Pt_0	Pd-b	−0.80	Pd-h	−1.15
			Pd-f	−1.32
Pt_1	PtPd-b	−0.85	PtPd-h	−1.17
			PtPd-f	−1.36
	Pd-b	−0.82	Pd-h	−1.16
			Pd-f	−1.33
Pt_2	Pt-b^e	−0.90	PtPd-h1	−1.11
			PtPd-f1	−1.33
	PtPd-b	−0.83	PtPd-h2	−1.08
			PtPd-f2	−1.28
	Pd-b	−0.82	Pd-h	−1.17
			Pd-f	−1.33
Pt_3	Pt-b^e	−0.81	Pt-h	−0.97
			PtPd-h1	−1.25
	PtPd-b	−0.79	PtPd-h2	−1.11
			PtPd-f1	−1.38
	Pd-b	−0.70	Pd-h	−1.20
			Pd-f	−1.27
Pt_4	Pt-b^r	−0.72	Pt-h	−0.91
			Pt-f	−1.18
	Pt-b^e	−0.78	PtPd-h1	−1.04
			PtPd-f1	−1.27
	PtPd-b1	−0.75	PtPd-h2	−1.22
			PtPd-f2	−1.31
	PtPd-b2	−0.75	Pd-h	−1.19
	Pd-b	−0.74	Pd-f	−1.25

Supplementary Table 2 | The adsorption energies (E_{ads}, given in eV) of molecular oxygen (O_2) and atomic oxygen (O*) on different adsorption sites corresponding to the model catalysts of the Pt_5 to Pt_8.

	O_2-site	E_{ads}	O*-site	E_{ads}
Pt_5			Pt-h	−0.92
	Pt-b^{r}	−0.68	Pt-f	−1.10
	Pt-b^{e1}	−0.79	PtPd-h1	−1.03
	Pt-b^{e2}	−0.73	PtPd-f1	−1.26
	PtPd-b1	−0.75	PtPd-h2	−1.12
	PtPd-b2	−0.65	PtPd-f2	−1.31
	Pd-b2	−0.72	Pd-h	−1.02
			Pd-f	−1.26
Pt_6			Pt-h	−0.93
	Pt-b^{r}	−0.63	Pt-f	−1.03
	Pt-b^{e}	−0.75	PtPd-f1	−1.27
	PtPd-b1	−0.79	PtPd-h1	−1.12
	PtPd-b2	−0.75	PtPd-f2	−1.40
	Pd-b	−0.68	Pd-h	−1.19
			Pd-f	−1.27
Pt_7			Pt-h	−0.87
	Pt-b^{r}	−0.62	Pt-f	−1.12
	Pt-b^{e}	−0.76	PtPd-h1	−1.03
	PtPd-b1	−0.74	PtPd-f1	−1.26
	PtPd-b2	−0.72	PtPd-h2	−1.14
	Pd-b	−0.71	PtPd-f2	−1.32
			Pd-h	−1.03
			Pd-f	−1.33
Pt_8			Pt-h	−0.88
	Pt-b^{r1}	−0.63	Pt-f	−1.06
	Pt-b^{r2}	−0.66	PtPd-h1	−1.06
	Pt-b^{e1}	−0.78	PtPd-f1	−1.28
	Pt-b^{e2}	−0.75	PtPd-h2	−1.14
	PtPd-b1	−0.77	PtPd-f2	−1.42
	PtPd-b2	−0.74	Pd-h	−0.96
	Pd-b	−0.64	Pd-f	−1.20

Supplementary Table 3 | The adsorption energies (E_{ads}, given in eV) of molecular oxygen (O_2) and atomic oxygen (O*) on different adsorption sites corresponding to the model catalysts of the Pt_9, Pt_{16}, Pt_{32} and pure Pt(111).

	O_2-site	E_{ads}	O*-site	E_{ads}
Pt_9	Pt-b^{r1}	−0.61	Pt-h	−0.96
	Pt-b^{r2}	−0.67	Pt-f	−1.06
	Pt-b^{e1}	−0.80	PtPd-h1	−1.11
	Pt-b^{e2}	−0.80	PtPd-f2	−1.30
	PtPd-b1	−0.77	PtPd-h2	−1.00
	PtPd-b2	−0.63	PtPd-f2	−1.29
	Pd-b	−0.65	Pd-h	−0.98
			Pd-f	−1.15
Pt_{16}	Pt-b	−0.67	Pt-h	−0.95
			Pt-f	−1.19
Pt_{32}	Pt-b	−0.71	Pt-h	−0.78
			Pt-f	−1.17
Pt(111)	Pt-b	−0.73	Pt-h	−0.88
			Pt-f	−1.29

Supplementary Table 4 | Reaction energy barrier (ΔE, given in eV) of the selected O_2 dissociation (ΔE1) and O* hydrogenation (ΔE2) pathways on the Co@Pd-Pt_n (n = 0-9, 16 and 32), Pd(111) and Pt(111) surface models.

	Pd	Pt_0	Pt_1	Pt_2	Pt_3	Pt_4	Pt_5	Pt_6	Pt_7	Pt_8	Pt_9	Pt_{16}	Pt_{32}	Pt
ΔE1	0.62	0.62	0.34	0.44	0.41	0.63	0.71	0.78	0.74	0.69	0.69	0.65	0.70	1.04
ΔE2	0.21	0.16	0.24	0.10	0.15	0.10	0.08	0.16	0.11	0.13	0.14	0.10	0.01	0.02

Supplementary Table 5 | Reverse reaction barrier (ΔE^R, given in eV) of the selected O_2 dissociation ($\Delta E1^R$) and O* hydrogenation ($\Delta E2^R$) pathways on the Co@Pd-Pt_n (n = 0-9, 16 and 32), Pd(111) and Pt(111) surface models.

	Pd	Pt_0	Pt_1	Pt_2	Pt_3	Pt_4	Pt_5	Pt_6	Pt_7	Pt_8	Pt_9	Pt_{16}	Pt_{32}	Pt
$\Delta E1^R$	1.84	1.88	1.57	1.60	1.49	1.72	1.69	1.84	1.66	1.72	2.23	1.66	1.42	2.55
$\Delta E2^R$	0.08	0.08	0.01	0.08	0.08	0.04	0.04	0.08	0.05	0.03	0.04	0.06	0.14	0.11

Supplementary Table 6 | The calculated spin magnetic moment of pure Pt, Pd and Co surface models. For comparison, the calculated magnetic moments per atom for bulk Pt, Pd and Co are showed as the values of μ_B.

	1st layer	2nd layer	3rd layer	4th layer	5th layer	6th layer	μ_B
Pt	0.00	0.00	0.00	0.00	0.00	0.00	0.00
Pd	0.25	0.38	0.38	0.38	0.38	0.25	0.31
Co	1.73	1.67	1.65	1.66	1.68	1.79	1.67

Supplementary Table 7 | The calculated magnetization of Pt_3, Pt_9 and Pt_{16} surface models. For Pt_3 model, the 3Pt/13Pd of the first layer represents the average magnetic moment of the three Pt atoms and the rest of the thirteen Pd atoms in this atomic layer, respectively (also applicable to Pt_9 model). Other Pt, Pd and Co represent the average magnetic moment corresponding to the one atomic layer from the top to the bottom layer within the 4×4 supercell, respectively.

	1st layer (Pt)	1st layer (Pd)	2nd layer (Pd)	3rd layer (Pd)	4th layer (Co)	5th layer (Co)	6th layer (Co)
Pt_3	0.29	0.28	0.32	0.29	1.81	1.66	1.37
Pt_9	0.23	0.24	0.28	0.28	1.77	1.58	1.18
Pt_{16}	0.23	0.30	0.30	0.27	1.74	1.50	0.98

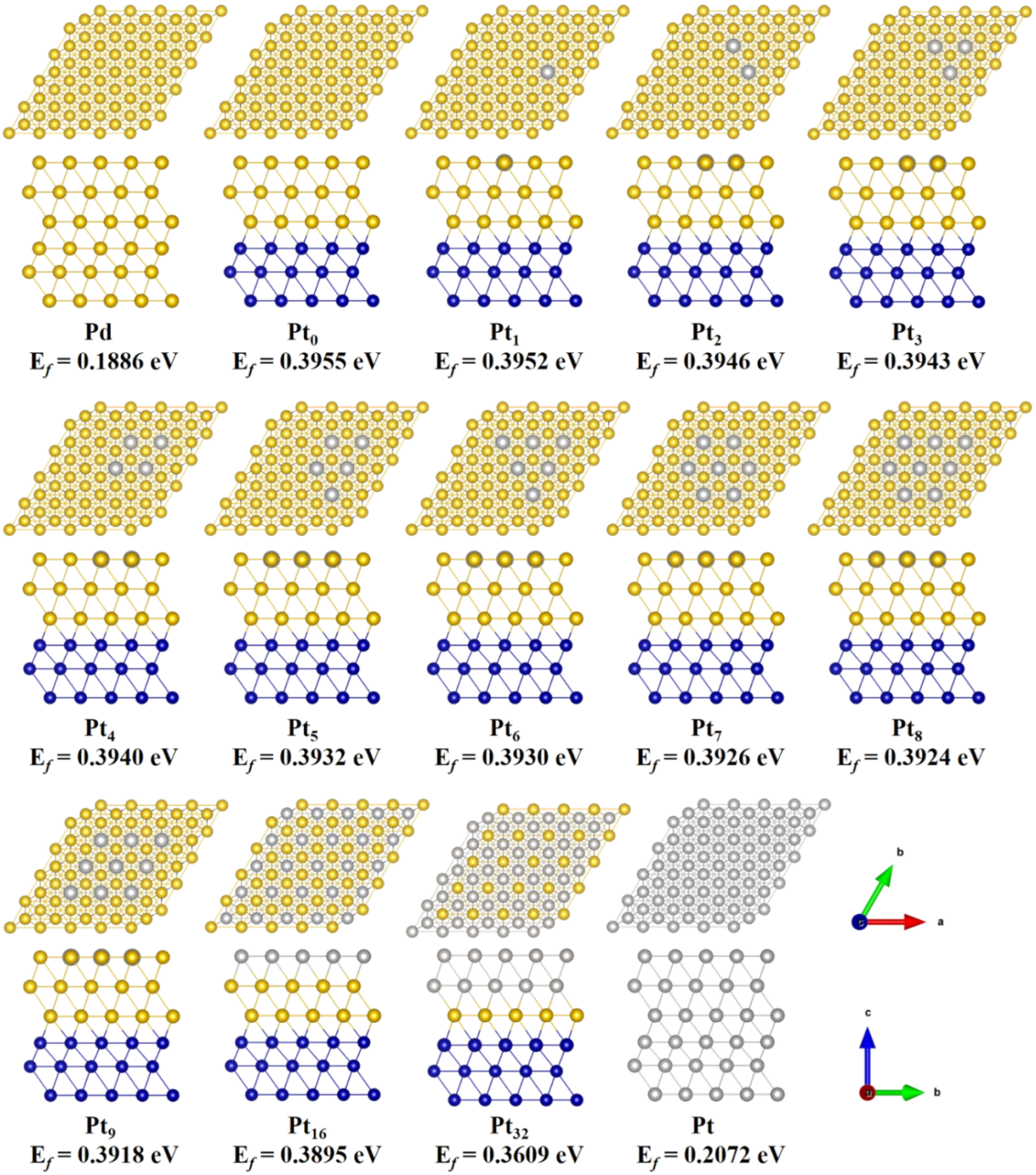

Supplementary Fig. 1 | Top and side views of the Co@Pd-Pt_n (n=0-9, 16 and 32), pure Pd and pure Pt surface models, which are composed of 6 atomic layers with 1st-3rd slabs as the shell layer and 4th-6th slabs as the core component, together with the calculated E_f of each configurations. The blue, yellow and grey balls represent Co, Pd, and Pt atoms, respectively.

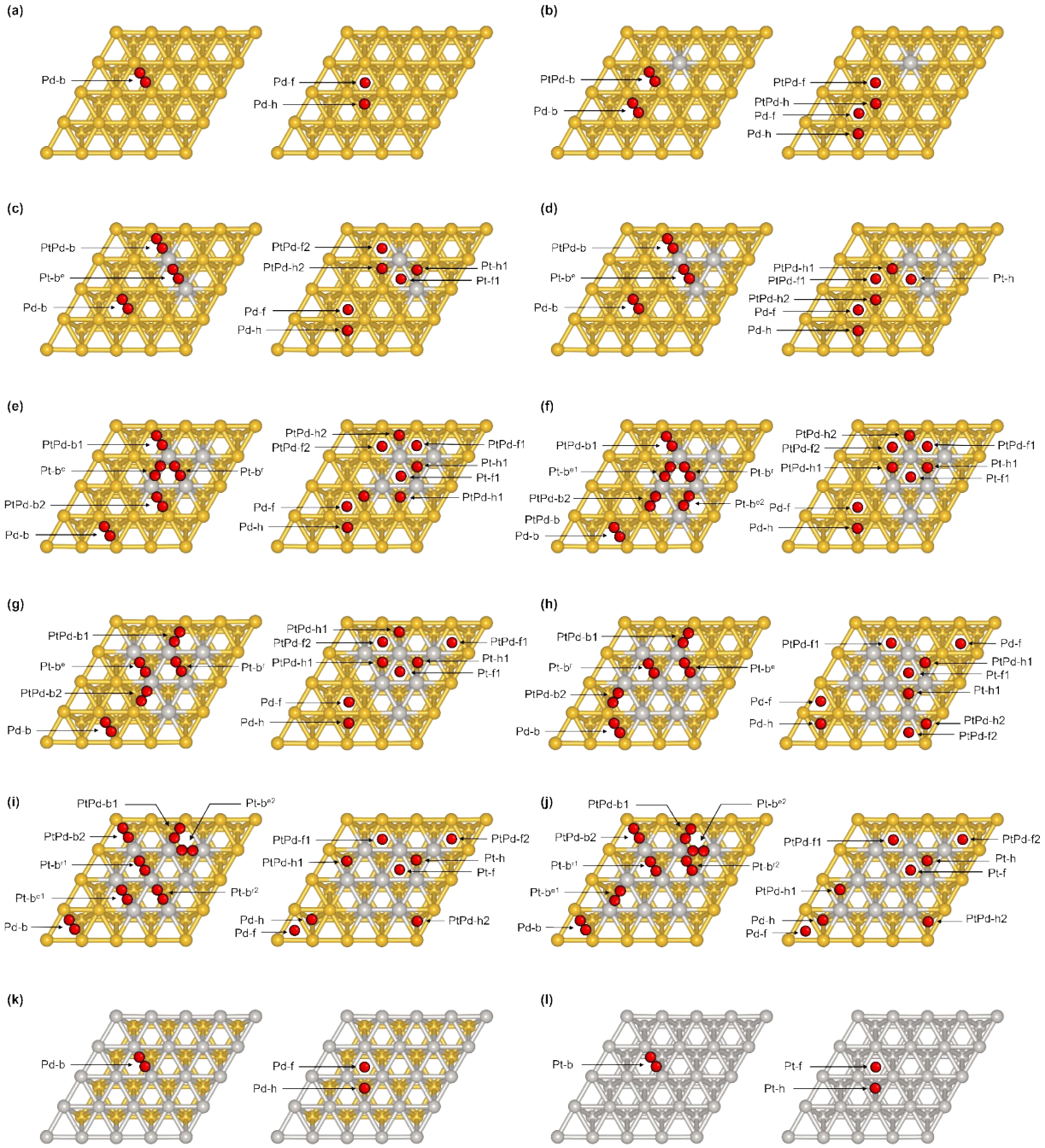

Supplementary Fig. 2 | Top views of the atomic adsorption structures of the O_2 (left) and O* (right) on (a) Pd(111) or Pt_{32}, (b) to (j) Pt_1 to Pt_9, (k) Pt_{16} and (l) Pt (111) surface models. The corresponding data is listed in Table S1. For clarity, only the top two-layer atoms of all the slabs are showed. The yellow, grey and red balls stand for Pd, Pt and O atoms, respectively. The hollow sites on the surface above the yellow/grey atoms and the vacancies correspond to the hcp sites and fcc sites, respectively.

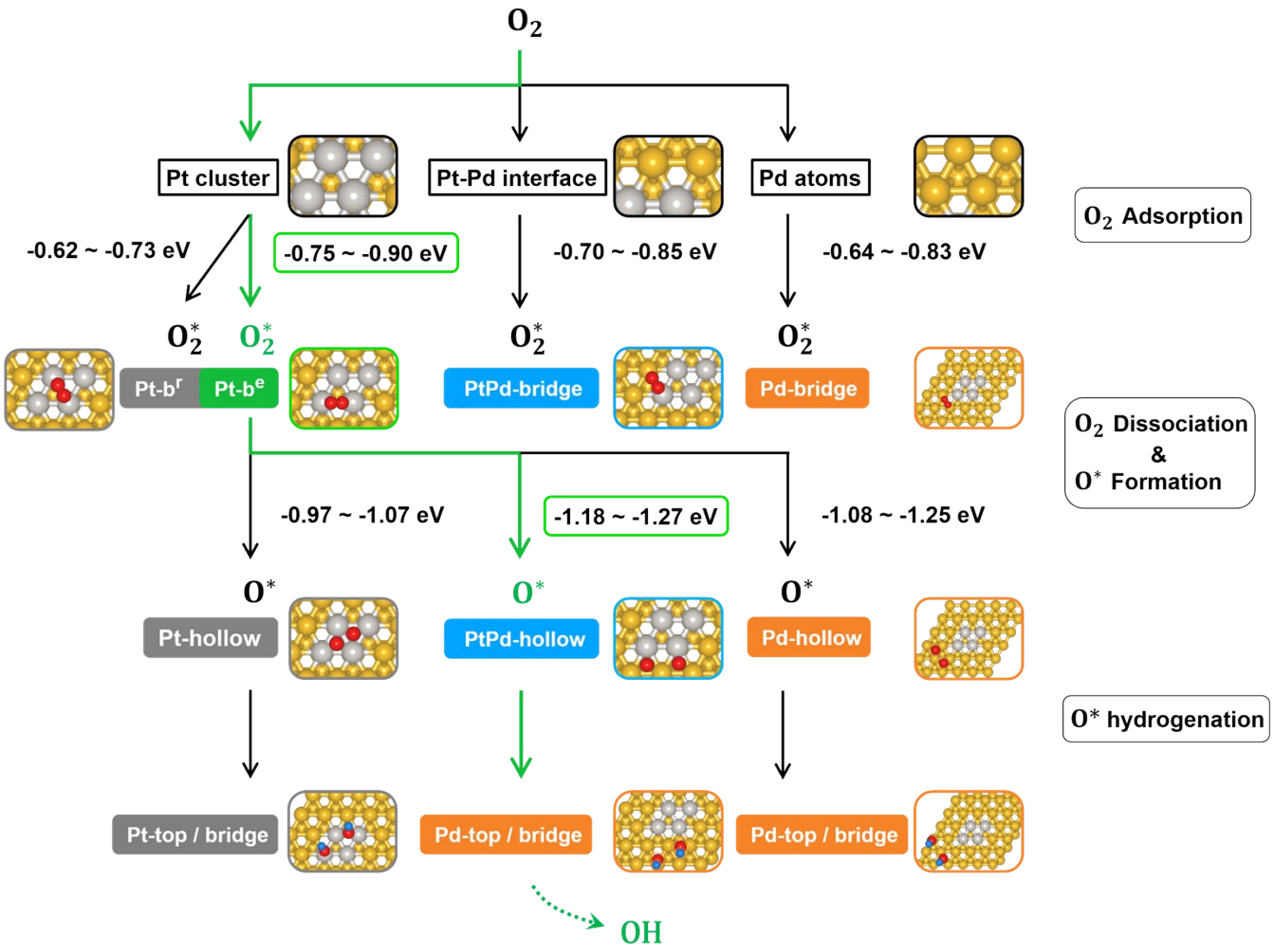

Supplementary Fig. 3 | The reaction scheme of the calculated E_{ads}–dependent oxygen conversion mechanism (highlight with green arrow line) across the different adsorption sites of the three regions on the Co@Pd-Pt_n systems in ORR. The chemical reactions in the illustration includes the O_2 adsorption, the most important O_2 dissociation / O* formation and O* hydrogenation. The superscript "*" denotes the adsorbed molecular O_2 or atomic O on catalyst surface; the yellow, grey, red and blue spheres respectively represent Pd, Pt, O and H atoms.

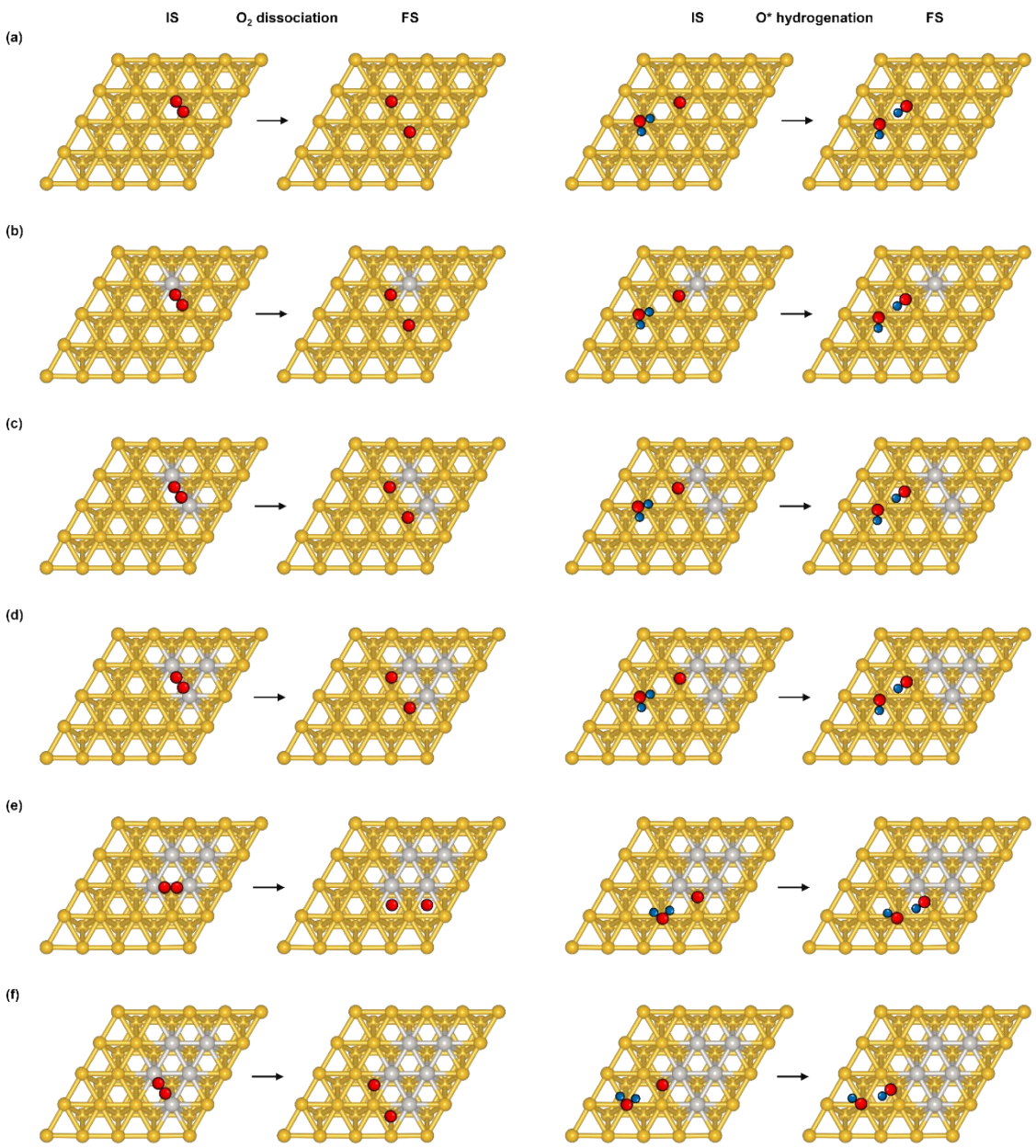

Supplementary Fig. 4 | Top view structures of selected O_2 dissociation and O* hydrogenation steps in ORR on various surface models, including (a) Pd(111) or Pt_{32}, (b) Pt_1, (c) Pt_2, (d) Pt_3, (e) Pt_4, and (f) Pt_5. The IS and FS respectively stands for the initial-state and final-state. The yellow, grey, red and blue spheres stand for Pd, Pt, O and H atoms, respectively. For clarity, only the top two-layer atoms of all the slabs are showed; the hollow sites above the yellow atoms and the vacancies correspond to the hcp and fcc sites, respectively

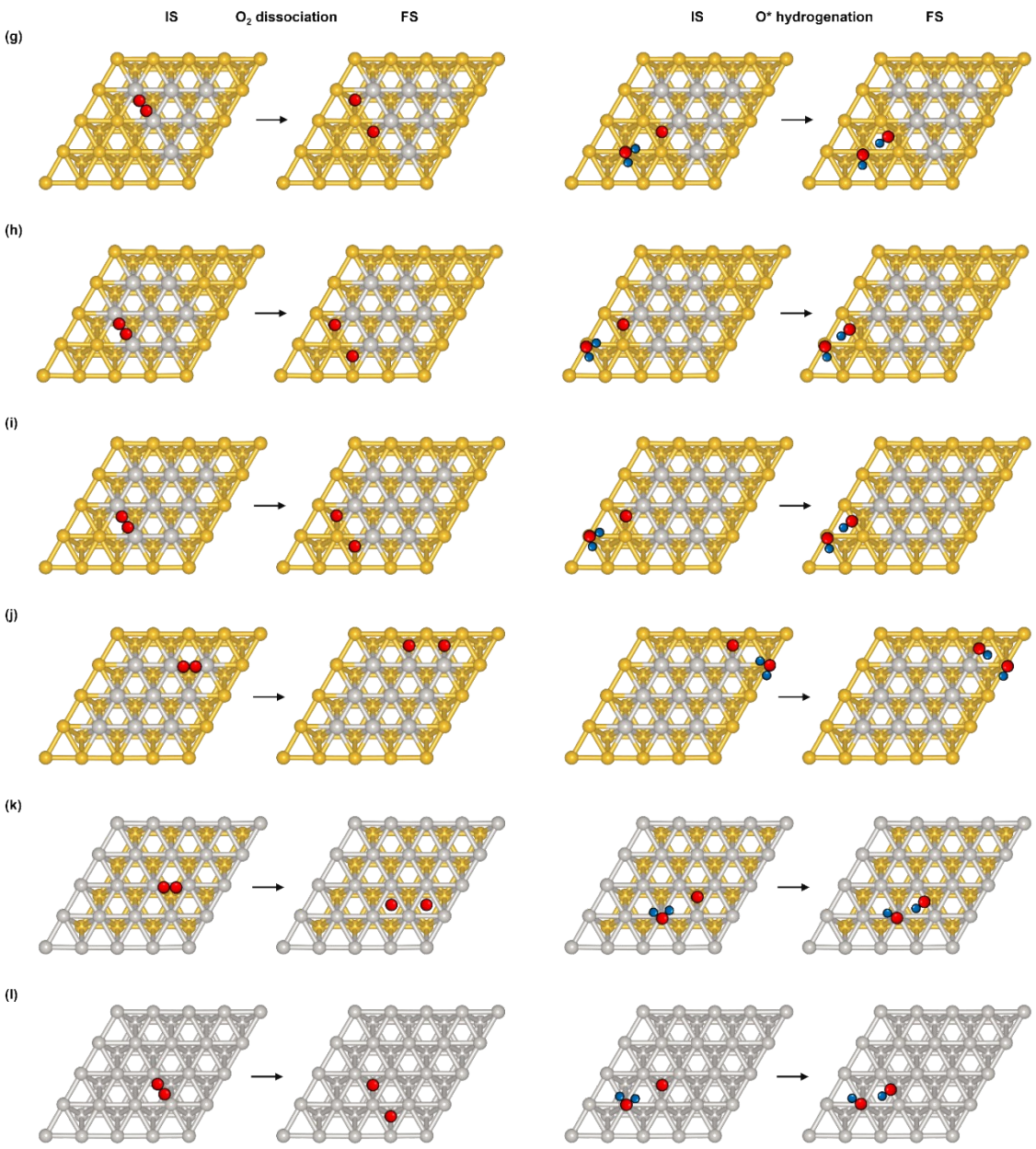

Supplementary Fig. 5 | Top view structures of selected O_2 dissociation and O* hydrogenation steps in ORR on various surface models, including (g) Pt_6, (h) Pt_7, (i) Pt_8, (j) Pt_9, (k) Pt_{16}, and (l) Pt(111). The IS and FS respectively stands for the initial-state and final-state. The yellow, grey, red and blue spheres stand for Pd, Pt, O and H atoms, respectively. For clarity, only the top two-layer atoms of all the slabs are showed; the hollow sites above the yellow/grey atoms and the vacancies correspond to the hcp and fcc sites, respectively

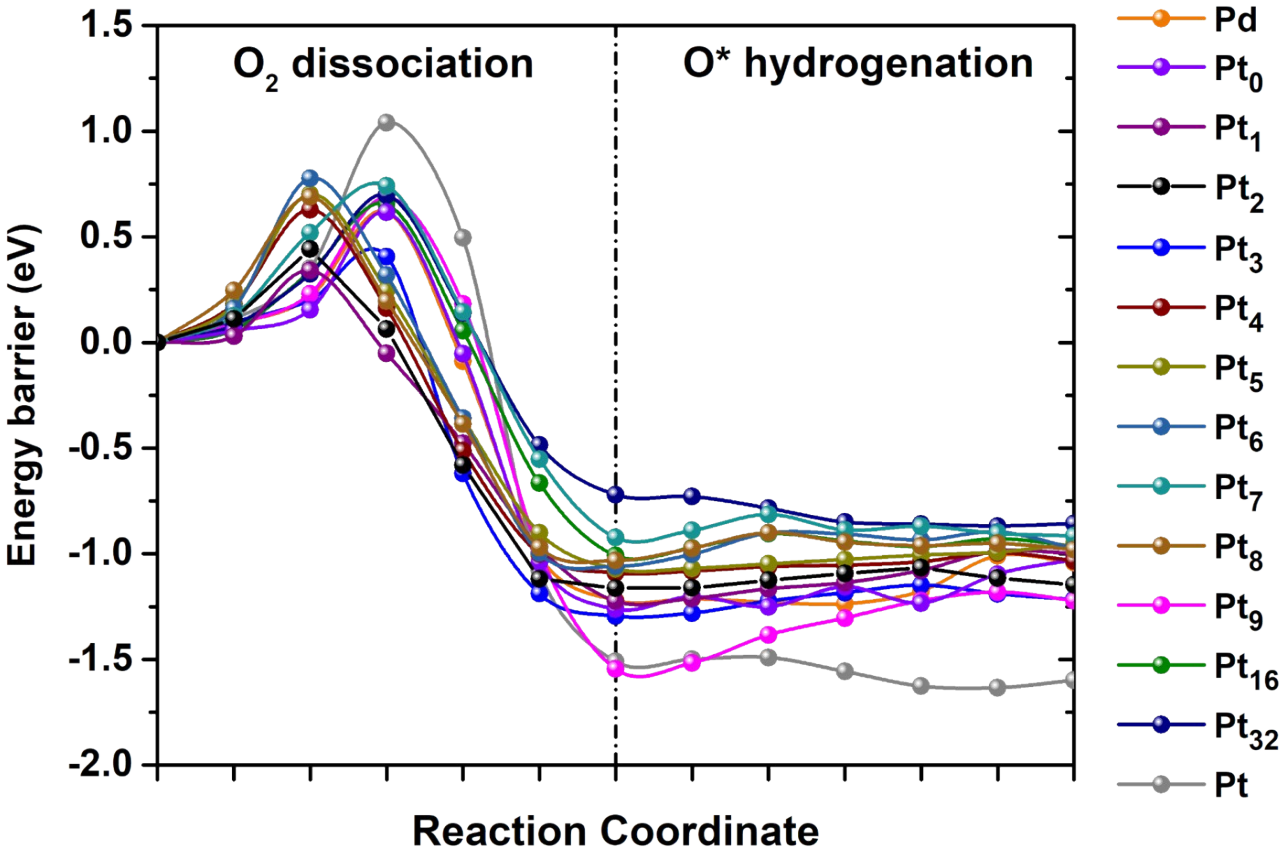

Supplementary Fig. 6 | Simulated reaction coordinates of selected first O_2 dissociation and subsequent O* hydrogenation pathways on the Co@Pd-Pt_n (n = 0-9, 16 and 32), Pd(111) and Pt(111) surface models. The corresponding transition-state (TS) value of each reaction path is listed as the ΔE in Table S1.

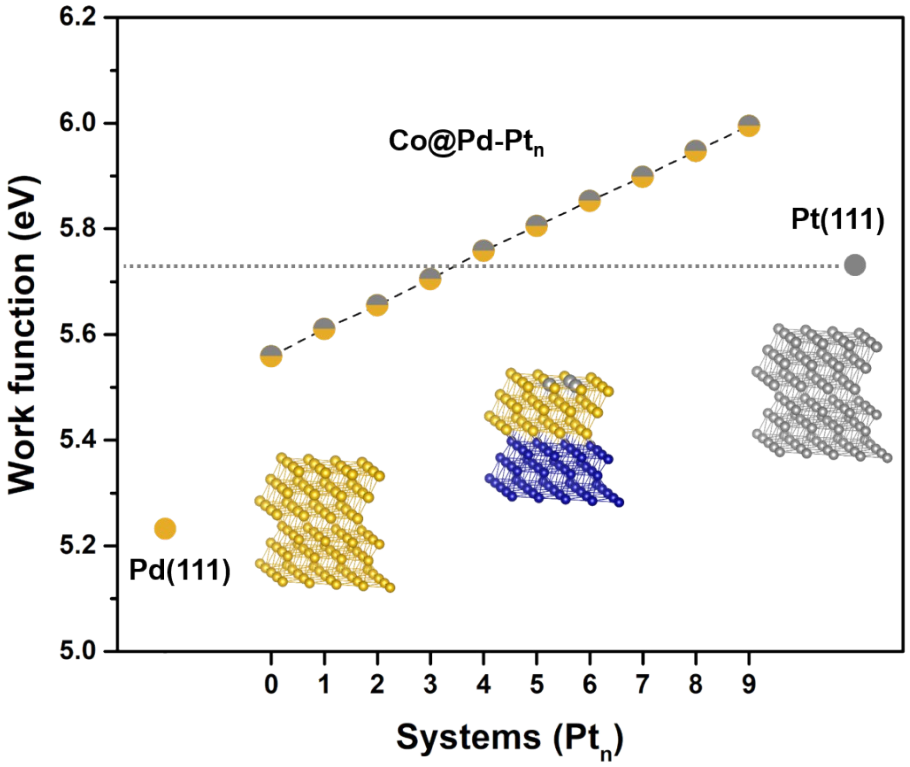

Supplementary Fig. 7 | Work function of different model systems, including Pd(111), Co@Pd-Pt$_n$ (n=0-9) and Pt(111).

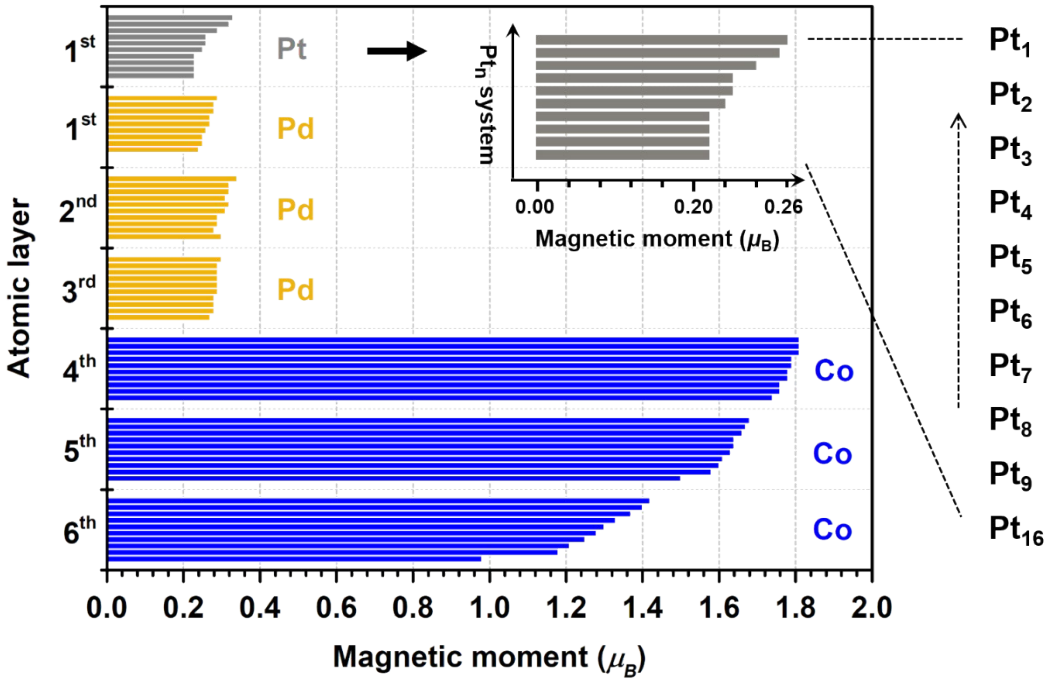

Supplementary Fig. 8 | Comparison of the average magnetic moments of Pt, Pd and Co atoms in each layer of the calculated 6-layer slab Pt_n models (n = 1-9 and 16). For clarity, the color bars corresponding to each atomic layer in the y-axis are the models from Pt_1 to Pt_{16} from top to bottom, the grey, yellow and blue bars represent Pt, Pd and Co atoms, respectively. There are two 1^{st} layers in the y-axis because in the Pt_n system, the first atomic layer (the outermost layer) contains both shell Pd atoms and doped Pt atoms.

Supplementary Note 2 | Detailed discussions for the magnetic variations of Pt, Pd and Co atoms located in different atomic layers inside the Co@Pd-Pt_n systems

To further reveal the spin coupling interactions between the surface cluster, shell layer and core regime inside the trimetallic systems, we calculated the layer-averaged spin magnetic moment of each model in comparison with the magnetic moment of bulk Pt, Pd and Co: see Supplementary Fig. S9 (the corresponding data are listed in Table S4 and S5). For brevity, only the representative Pt_3, Pt_9 and Pt_{16} of the Pt_n models are selected to be investigated in the magnetization calculation to demonstrate the correlation of electronic coupling between different elements in the Pt_n systems.

It is notable that for the Pt atoms of the three ternary models, all of the calculated magnetic moments (in the range of 0.23–0.29 μ_B) are conspicuously higher than that of bulk Pt (0.0 μ_B), which can be attributed to the spin coupling between Pt atoms of surface clusters and their neighboring Pd atoms of the shell layer. Furthermore, the average spin magnetic moment of Pt atoms for Pt_3 (0.29 μ_B) is higher than that of Pt_9 (0.23 μ_B) and Pt_{16} (0.23 μ_B). Meanwhile, for Pt_3, the average magnetic moments of the deepest three Co layers are also higher than that of Pt_9 and Pt_{16} (for data see Table S5). However, for the Pd atoms in the upper three layers, the spin magnetic moments per layer for the Pt_3, Pt_9 and Pt_{16} models are basically the same (~ 0.3 μ_B) and of the same magnitude as that of the calculated bulk Pd (0.31 μ_B), implying that the Pd shell-layer can be considered as relatively spin-insensitive.

Therefore, the results provide evidences that the spin coupling interaction between the Pt cluster, Pd shell layer and Co core is existed in our trimetallic systems to trigger an obvious magnetization enhancement of topmost Pt atoms embedded into Pd surface, which is likely to cause the charge coupling (redistribution) and DOS variation throughout the whole systems. Especially, the Pt atoms in the smallest trimer-cluster of Pt_3 exhibits the largest change in magnetic moment, i.e., the strongest electron coupling with other heteroatoms, compared to the P_9 and Pt_{16}.

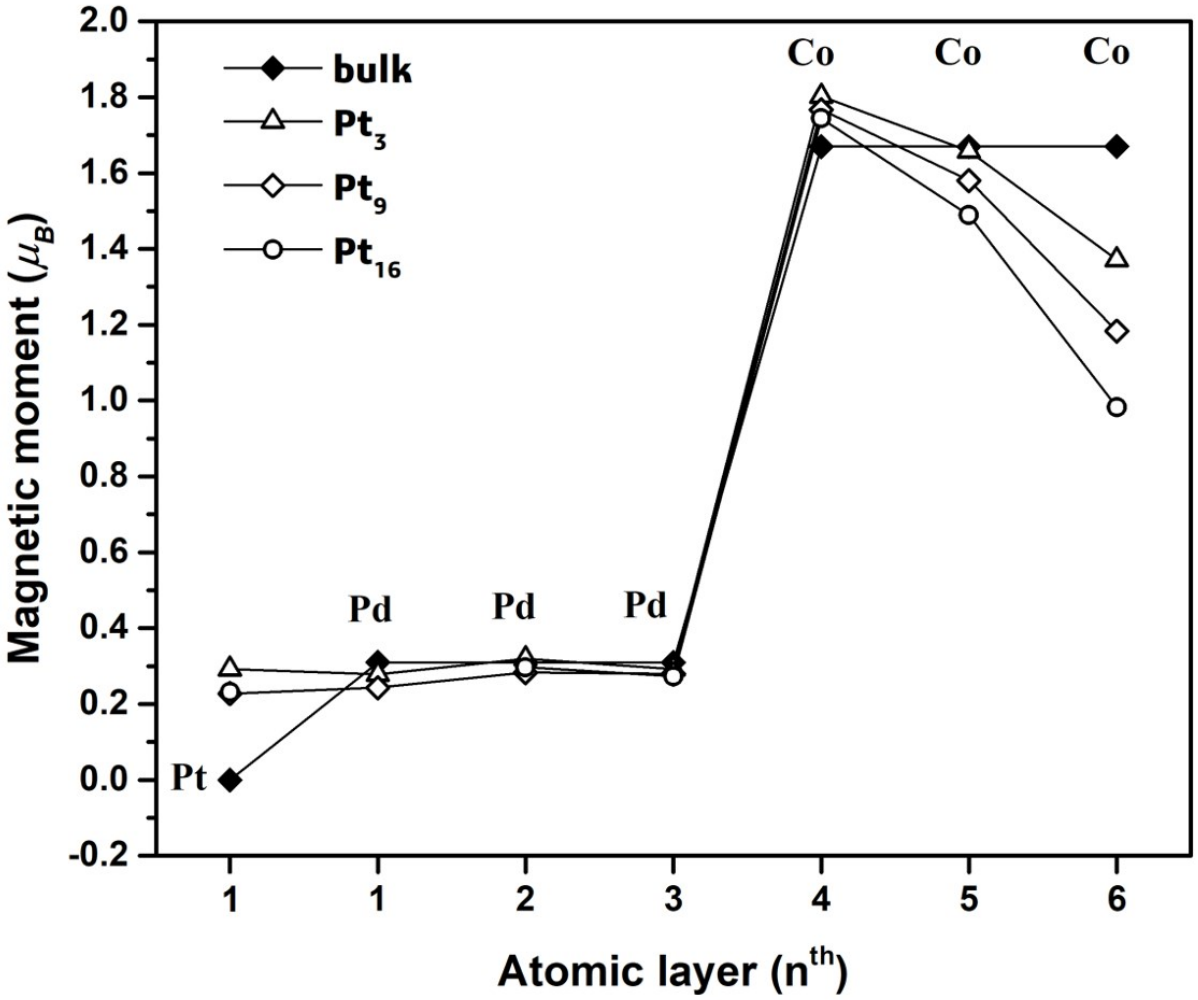

Supplementary Fig. 9 | Calculated magnetization of the different bulk and 6-layer slab models. The fulfilled symbols denote the bulk magnetic moment of Pt, Pd and Co (unit in $\boldsymbol{\mu_B}$, data see Table S7) corresponding to the 1st layer, 1st-3rd layers and 4th-6th layers, respectively. The hollow triangle, rhombus and circle are denoted as each layer's average magnetic moment of Pt_3, Pt_9 and Pt_{16} surface models corresponding to the Table S7. The respective ternary model structures see supplementary Fig. 1.